



Adsorption characteristics and mechanisms of bisphenol A on novel nitrogen-modified biochar derived from waste masks and biomass

Tongtong Wang¹ · Dalal Z. Husein³ · Siyan Guo² · Xinle Zhang² · Jiarui Kang² · Huixia Wang² · Shumiao Cao² · Zhonghua Shangguan⁴ · Hui Shi^{1,2}

Received: 1 February 2024 / Accepted: 30 July 2024 / Published online: 6 August 2024
© The Author(s), under exclusive licence to Springer-Verlag GmbH Germany, part of Springer Nature 2024

Abstract

Resource utilization of waste masks has become an urgent scientific issue. In this work, with sustainably, waste masks and biomass were co-pyrolysis with oxygen limitation to prepare mask-based biochar (MB). Then, urea was introduced to prepare novel nitrogen modified mask-based biochar (NMB) via a one-step hydrothermal synthesis method. The adsorption characteristics of NMB on the emerging environmental pollutant, bisphenol A (BPA), were evaluated via batch adsorption tests. Moreover, the physicochemical properties of the materials were characterized with various advanced techniques. Also, the roles of waste masks and nitrogen modification were explored. The adsorption mechanisms of NMB on BPA were revealed as well as the performance differences between different adsorbents. The results showed that waste masks participated in thermochemical reactions, shaped the microsphere structure of biochar, and increased the types of surface functional groups. The nitrogen modification enriched the surface elemental composition and activated the specific surface area via the mesopore. These would enhance the adsorption performance. The maximum adsorption of BPA by NMB was $62.63 \text{ mg}\cdot\text{g}^{-1}$, which was approximately 2.35–5.58 times higher than that of the control materials. Temkin model and pseudo-second-order model optimally simulate the isothermal and kinetic adsorption, respectively. The adsorption mechanisms are jointly by physical and chemical adsorption, which mainly includes π - π interaction, hydrogen bonding, intraparticle diffusion, surface adsorption, and ion exchange. After discussion and evaluation, NMB has lower preparation process cost ($7.21 \text{ USD}\cdot\text{kg}^{-1}$) and safety, with potential for environmental applications. This study aims to expand new ideas for the comprehensive utilization of waste masks and the preparation of eco-friendly materials. Moreover, it provides a theoretical basis for the removal of BPA.

Keywords Waste masks · Biochar · Nitrogen modification · Bisphenol A · Adsorption mechanisms · Cost and risk evaluation

Introduction

The global outbreak of coronavirus disease 19 (COVID-19) has become the most impactful epidemic on record. To prevent this pandemic virus from posing a serious additional threat to humans, the World Health Organization (WHO) has proposed some policy responses. For example, the proposal to wear disposable medical masks (DMMs) indoors and outdoors to reduce the spread of COVID-19 in the population (Desai and Aronoff 2020). Many countries have implemented mandatory requirements for the wearing of DMMs in public places (Saberian et al. 2021). According to the Chinese magazine National Geographic, it was predicted that nearly 129 billion DMMs were consumed globally per month during the COVID-19 epidemic, with 1.8 to 2.2 billion per day consumed in Asia alone (Luo et al. 2021; Yuwen

Responsible Editor: Tito Roberto Cadaval Jr

✉ Hui Shi
shihui@xauat.edu.cn

- ¹ Institute for Interdisciplinary and Innovate Research, Xi'an University of Architecture and Technology, Xi'an 710055, People's Republic of China
- ² School of Environmental and Municipal Engineering, Xi'an University of Architecture and Technology, Xi'an 710055, People's Republic of China
- ³ Chemistry Department, Faculty of Science, New Valley University, El-Kharja 72511, Egypt
- ⁴ Xi'an Geological Survey Center, China Geological Survey, Xi'an 710054, People's Republic of China

et al. 2022). Such statistics continue to grow over time, with over 100 billion masks discarded into the environment due to use by 2023, creating a serious burden. Waste DMMs entering the environment have evolved into a new type of hazardous solid waste as they release microfibers and microplastics, also forming aerosols that may affect the global climate (Yuwen et al. 2022). It may take up to 450 years for these waste DMMs to decompose naturally (Wang et al. 2022). Therefore, the proper handling of waste DMMs has become an urgent scientific problem, which is beneficial to both human health and environmental protection.

Today, most waste DMMs cannot be recovered or chemically recycled, even if they are discarded correctly (Yuwen et al. 2022). The common disposal methods of waste DMMs are landfill and incineration, which unfortunately could easily lead to the release of toxic secondary pollutants and a high risk of virus transmission (Luo et al. 2021). This has compelled scholars to explore more eco-friendly and high-quality ways to utilize the resources of waste DMMs. Among many chemical treatments, the pyrolysis method under an inert atmosphere provides a green, cheap, and reliable disposal process (Wang et al. 2022). Luo et al. (2021) found that the method not only kills potential viruses but also converts waste masks into functional carbon materials and high-quality bio-oil. This is because DMMs are essentially composed of polymers (e.g., polypropylene, polyester fibers) and metal nose clips (Oginni 2022). The polymers in the masks have the potential for the preparation of carbon-based materials, which has been confirmed by relevant research reports (Emenike et al. 2022; Li et al. 2023a). Simultaneously, polymer pyrolysis is typically a random cracking, where the breaking of chemical bonds leads to the random production of a quantity of low molecular hydrocarbons (Yuwen et al. 2022). This in turn generates bio-oils and pyrolysis gases. Oginni (2022) discussed the possibility of converting DMMs into high value-added bioproducts via oxygen-limited pyrolysis, which is one of the important thermo-chemical conversion technologies. Li et al. (2023a) sterilized and converted DMMs into carbon dots via a facile hydrothermal synthesis, which was applied to achieve good results in the spectroscopic detection of sodium sulfite and Fe^{3+} . To reduce energy consumption and enhance material properties, Emenike et al. (2022) proposed the co-pyrolysis of waste DMMs and leaves to prepare biochar, which was recommended as a possible adsorbent. However, the related research is still in the initial stage. What is the adsorption performance of co-pyrolysis-prepared mask-based biochar? What is the effect on environmental applications? All of them need to be explored in depth. Additionally, it is not clear what role the waste DMMs play in the structure of the biochar. Even the research on whether mask-based biochar may be modified like carbon materials and thus enhance the adsorption properties has not been reported. Therefore, there

is an urgent need to answer these questions and to further research the resource utilization of waste DMMs.

Bisphenol A (BPA, $\text{C}_{15}\text{H}_{16}\text{O}_2$) is a representative endocrine disruptor often employed in the production of polycarbonate and epoxy resins, which is widely applied to plastic products, food, and fine chemicals (Zhang et al. 2023). As an emerging environmental pollutant, BPA has been detected in a wide range of water bodies (Shi et al. 2022). Residual BPA has obvious harmful effects, such as disrupting the endocrine system, causing reproductive disorders, or inducing cancer (Xu et al. 2023). BPA is difficult to degrade rapidly owing to its antioxidant properties; thus, using an easy-to-operate adsorption method may be the first choice (Bi et al. 2020; Zhang et al. 2023). Therefore, this work will attempt to prepare mask-based biochar (MB) from waste DMMs by co-pyrolysis with cow dung under inert gas. Additionally, the enriched N-modified mask-based biochar (NMB) was prepared by hydrothermal synthesis using urea. This work also used advanced characterization techniques to analyze the basic physicochemical properties of the prepared materials and the role of the waste mask in the material structure. The batch adsorption experiments of the prepared materials on BPA were systematically investigated, and the experimental data were fitted with the classical adsorption models to elucidate the adsorption characteristics. The adsorption mechanisms and comparative adsorption performance of BPA by NMB have also been deeply explored. Finally, the risk of environmental applications and preparation costs for NMB were evaluated. This work is in line with the green development concept of “turning waste into valuable, and treating waste with waste.” The research highlights of this work are focused on exploring the possibility of comprehensive utilization of waste masks using co-pyrolysis, assessing the risk of environmental applications and preparation costs. The possible contribution is to expand the idea of preparing new waste mask-based eco-friendly material and to provide a theoretical basis for the removal of emerging pollutants.

Materials and methods

Chemical reagents and instruments

The waste DMMs (mainly composed of polypropylene and polyester fibers) were purchased from the market and used during the epidemic. Cow dung was taken from a dairy factory in Zhouzhi County, Xi'an City. These raw materials need to be cut and dried. The chemical reagents mainly involved bisphenol A (BPA), urea ($\text{CH}_4\text{N}_2\text{O}$), NaOH, KBr, and ethanol, all of which were analytically pure. They purchased from Shanghai Aladdin Biochemical Science and Technology Co. All chemical reagents do not require further purification, and the experimental water is ultrapure water.

Materials preparation

A certain mass of dried DMMs and cow dung (1:1, based on the screening of various composite ratios in pre-tests) were weighed and mixed well into an alumina crucible. And then put into a box-type atmosphere furnace (GF11Q-B type, Nanjing Boyuntong Instrument Company) with nitrogen pyrolysis throughout the whole process. The multi-stage program heating was adopted. The pyrolysis temperature was set at 450 °C for a constant temperature time of 3 h, and the heating rate of 5 °C·min⁻¹. The reaction mixture was naturally cooled to room temperature after the end of the reaction process. The solid obtained was ground through an 18-mesh sieve, i.e., the mask-based biochar prepared by co-pyrolysis, abbreviated as MB. Moreover, the precursor materials, pure mask biochar (MB₀) and pure cow dung biochar (CB), were prepared according to the same conditions.

Accurately weighed 3 g of the above MB and 1 g of urea (as a source of N modification) into a 250-mL beaker and added 100 mL of ultrapure water for magnetic stirring for 30 min. Subsequently, the mixture was ultrasonicated for 2 h (parameter, 50 °C and 40 kHz). The mixture was then transferred to a SLM 250 miniature hydrothermal reactor (Beijing Shijisenlang Experimental Instrument Co., Ltd.) with a controlled filling ratio of 80%. The temperature was slowly increased from room temperature to 200 °C and kept for 10 h. After the reaction was finished, the solution was naturally cooled to room temperature. Finally, the solution was pumped through a 0.22- μ m filter membrane and then dried at 80 °C to obtain nitrogen-modified mask-based biochar (NMB). The simplified synthesis route is illustrated in Fig. 1.

Characterization

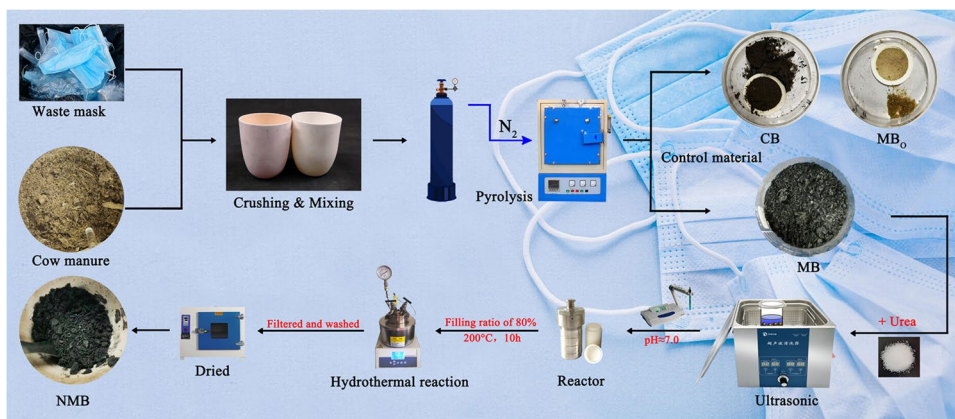
The element contents of C, N, H, and S were measured using a UNICUBE elemental analyzer (Elementar Co. Ltd., Berlin, Germany). The pH was measured by a PHS-3C pH meter

(Malvern Panalytical Ltd., Shanghai, China). The surface morphology of the materials was analyzed in a GeminiSEM 500 high-resolution field emission scanning electron microscope (FESEM, Carl Zeiss AG, Oberkochen, Germany), which was loaded with an X-MAXEDS spectroscopic detection system (EDS, Oxford Instruments, Oxford, UK). The BET-specific surface area (S_{BET}) and pore size analysis were determined using N₂ as the adsorbate, for which an ASAP 2460 analyzer (Micromeritics Instruments Co., Norcross, USA) was used. The materials were scanned with an Escalab 250 Xi X-ray photoelectron spectrometer (XPS, Thermo Fisher Scientific Co., Ltd., MA, USA) to investigate the chemical state of the main elements. The mineral species of the materials were identified using a D-MAX 2500 X-ray powder diffractometer (XRD, Rigaku Co., Ltd., Wilmington, USA). The infrared spectra (FTIR) were measured with KBr pellet methods using a Vertex70 FTIR spectrometer (Bruker Co., Ltd., Billerica, USA) over a range of 400–4000 cm⁻¹ with a resolution of 2 cm⁻¹. FTIR was used to analyze the surface functional groups of the sample. The zeta potential was determined using a Zetasizer Nano ZS90 (Malvern Panalytical Ltd., USA). The contact angle was determined using an OCA20 contact angle meter (Dataphysics Ltd., Germany).

Batch experiments

This study was carried out with reference to the classical batch adsorption experiments (Wang et al. 2017; Tang et al. 2022). The BPA solution contained 1 mL of anhydrous ethanol as a solvent to dissolve completely at room temperature (25 °C), and the solution pH was adjusted to approximately neutral with dilute NaOH. Adequate conical flasks were taken and 50 mL of BPA solution (10 mg·L⁻¹) and 0.05 g of the prepared materials were added separately and placed in a gas-bath thermostatic oscillator (240 rpm) for 24 h at 25 °C. The mixture was centrifuged at high speed for solid-liquid separation, and the solid filtrate was dried at 80 °C for

Fig. 1 Nitrogen-modified mask-based biochar preparation procedures



24 h and recovered to analyze the adsorption mechanisms. The filtrate was stored in reagent bottles under refrigeration (4 °C) and sealed from light, and then used to analyze the concentration of adsorbents after dilution. Three parallel replicates were assigned to each treatment, together with control and blank treatment. The statistical methods were applied to take the mean values for the subsequent analysis. Additionally, BPA concentration was determined on a Shimadzu Nexera UHPLC LC-30A ultra-high-performance liquid chromatograph. The adsorption capacity (Q_e , mg·g⁻¹) and removal rate (R_e , %) at equilibrium were calculated as follows:

$$Q_e = (C_0 - C_e) \frac{V}{m} \quad (1)$$

$$R_e = \left(1 - \frac{C_e}{C_0}\right) \times 100\% \quad (2)$$

where C_0 and C_e are the initial and equilibrium concentrations (mg·L⁻¹), respectively. m is the mass of added adsorbent (g) and V is the solution volume (L). The detailed operation of the batch experiments is described below. (1) Isothermal adsorption: the initial BPA concentrations were established at 1, 2, 5, 10, 15, 20, 25, 50, 100, 200, and 300 mg·L⁻¹, respectively. (2) Adsorption kinetics: the adsorption times of BPA were established at 5, 10, 30, 60, 120, 180, 300, 480, 720, 900, 1440, and 2160 min, respectively. Other settings were the same as the batch experiment above.

Moreover, the risk of possible release of organic pollutants from the materials MB₀, MB, and NMB was also briefly evaluated in this study via organic leaching tests: the leaching test method was referred to in the literature (Wang et al. 2021a; 2024) and the test instrument was a gas chromatograph mass spectrometer (GC-MS, TRACE 1300/ISQ 7000, Thermo Fisher Scientific, USA).

Adsorption models and data analysis

The experimental data were statistically analyzed using SPSS 26.0 (IBM Corporation, Armonk, USA). To better investigate the characteristics of the adsorption, four isotherm models (Langmuir, Freundlich, Temkin, and Dubinin-Radushkevich) and four adsorption kinetic models (pseudo-first-order, pseudo-second-order, Elovich, and intraparticle diffusion) were used in this work (Qiang et al. 2023; Al-sareji et al. 2024a). The detailed model expressions and the physical meanings represented by the parameters in each model are shown in the Supplementary Material (Table S1). Isothermal adsorption and adsorption kinetic curves were fitted and plotted using OriginPro 2018b (OriginLab, Northampton, USA).

Results and discussions

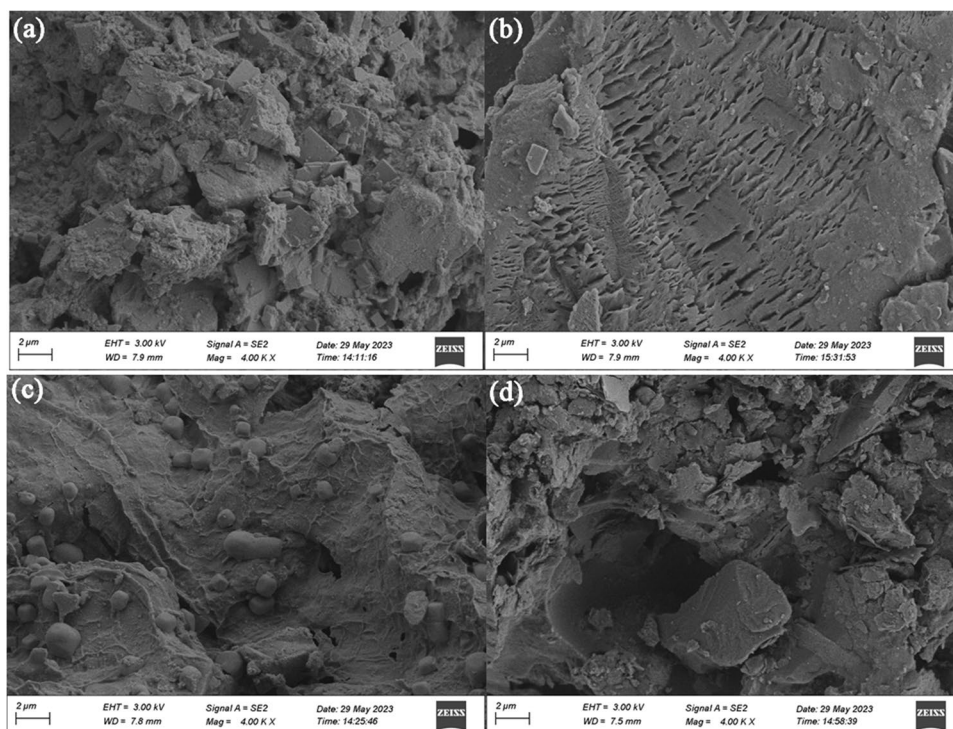
Characterization

To investigate the physicochemical properties of the materials, a variety of material characterizations are performed. These mainly include surface morphology and elemental analysis, crystal structure, surface functional groups, specific surface area and pore size analysis, zeta potential, and contact angle.

FESEM and surface elemental analysis

The FESEM of the prepared materials is presented in Fig. 2. MB₀ consists of many irregular particle accumulations (Fig. 2a), which may be the esters produced by the co-pyrolysis reaction of polymers in the waste DMMs. Some of the flaky or square particles may be polypropylene or other crystals in the waste DMMs (Emenike et al. 2022; Yuwen et al. 2022). Figure 2b shows that the CB surface exhibits fish scale-like pores and retains a fiber structure, which is typical of porous materials. Figure 2c displays that MB has a textured structure from the cow dung biochar possessed. The cow dung-specific fibers undergo co-polymerization reaction with the mask polymer, which may produce spherical projections and be widely distributed on the MB surface (Emenike et al. 2022). This implies that mask polymers (such as polypropylene and polyester fibers) may react thermochemically with biomass (hemicellulose, cellulose, and lignin) via thermal polycondensation and cleavage (Zhang et al. 2020), shaping the micro-spherical particles (Luo et al. 2021; Oginni 2022). Figure 2d demonstrates that the microsphere structure on the surface disappears with N modification, producing many tiny flakes and granular particles that fluff up the NMB. This indirectly indicates that N modification plays a role in activating the surface structure of the biochar and boosting its volume. Additionally, urea may react with MB under hydrothermal conditions, leading to the fragmentation of the microspheres (Qiang et al. 2023). The EDS results are shown in Fig. 3. It could be noticed that the O element content on the surface of NMB was significantly increased, and the N element content was slightly increased, while the C and other element contents were also significantly reduced. This intuitively explains the success of N-modified biochar, especially the enhanced O and N content, which may facilitate the binding reaction at multiple adsorption sites (Tang et al. 2022). Furthermore, this study quantitatively determined the important elemental content of NMB and MB using an elemental analyzer (CHNS mode), and the results are

Fig. 2 FESEM of the prepared materials (magnified 4000 times): **a** for MB₀, **b** for CB, **c** for MB, and **d** for NMB



shown in Table 1. It is observed that the N element content in NMB is significantly higher than in MB. This is favorable for activating the surface-active sites and potentials of the material to remove pollutants, as the higher electronegativity of the N atom (3.04) than that of the C atom (2.54), which allows for altered electron transfer and affects the electron spin properties of the biochar surface (Qiang et al. 2023). Furthermore, a relative decrease in the content of C, H, and S elements in NMB relative to MB could be found, which is similar to the EDS results (Fig. 3). In particular, the decrease in the content of heteroatoms such as element S could be attributed to the removal of impurities in the material by N modification, which helps to enhance the surface properties.

XRD and FTIR analysis

Figure 4a shows an XRD diffractogram demonstrating the physical phase structure contained in the prepared materials. The crystals with 2θ located at 26.4° were found to be graphitic carbon (JCPDS No. 41–1487) by Jade 6.5 software and standard material card analysis of the International Centre for Diffraction Data. This diffraction peak is considered to be characteristic of biochar as a carbon material (Wang et al. 2021b). Moreover, the crystals were also matched in both NMB and control materials, implying that the corresponding biochar was prepared in this study. Specifically, the graphitic carbon diffraction peaks were more pronounced in the MB and NMB prepared via co-pyrolysis compared

to CB and MB₀, suggesting that co-pyrolysis of the waste masks with biomass may undergo further thermochemical reactions to enhance the crystallinity (Emenike et al. 2022; Oginni 2022). Also, this shapes the microsphere structure as demonstrated in Fig. 2c. Additionally, substances such as polypropylene, polyethylene, polyethylene terephthalate, and ketone miscellaneous peaks were found in MB₀, MB, and NMB, which are closely related to the organic polymers in waste DMMs. Notably, residual urea (JCPDS No. 72–0118) crystals were also found near 22.1° and 35.4° for NMB, implying the feasibility of the N-modified MB preparation method.

Figure 4b shows the FTIR (processed with baseline calibration) aimed at illustrating the surface functional groups of the prepared materials (Li et al. 2023b). Overall, all materials have similar characteristic peaks, which include hydroxyl stretching vibrational peaks ($-\text{OH}$) near 3426 cm^{-1} , C-H stretching vibrational peaks (e.g., $-\text{CH}_3$) near 2922 cm^{-1} , amino vibrational peaks ($-\text{NH}_2$) near 1606 cm^{-1} , aromatic acidic vibrational peaks ($-\text{COOH}$) near 1437 cm^{-1} , C-C (or C=C) vibrational peaks near 1020 cm^{-1} , and heterocyclic functional groups of aromatic compounds near $400\text{--}800\text{ cm}^{-1}$ (Wang et al. 2021a). The characteristic peak of MB₀ at 1560 cm^{-1} may be the amino vibrational peaks ($-\text{NH}_2$), which is red-shifted at NMB to near 1606 cm^{-1} with co-pyrolysis and N modification (Wang et al. 2021b). Moreover, based on the chemical composition of the waste masks, the characteristic peak at 1560 cm^{-1} has a lower probability of being nitrogen oxides. This is mainly due to the pyrolysis of

Fig. 3 EDS surface elemental analysis of the prepared materials: **a** for MB, **b** for NMB

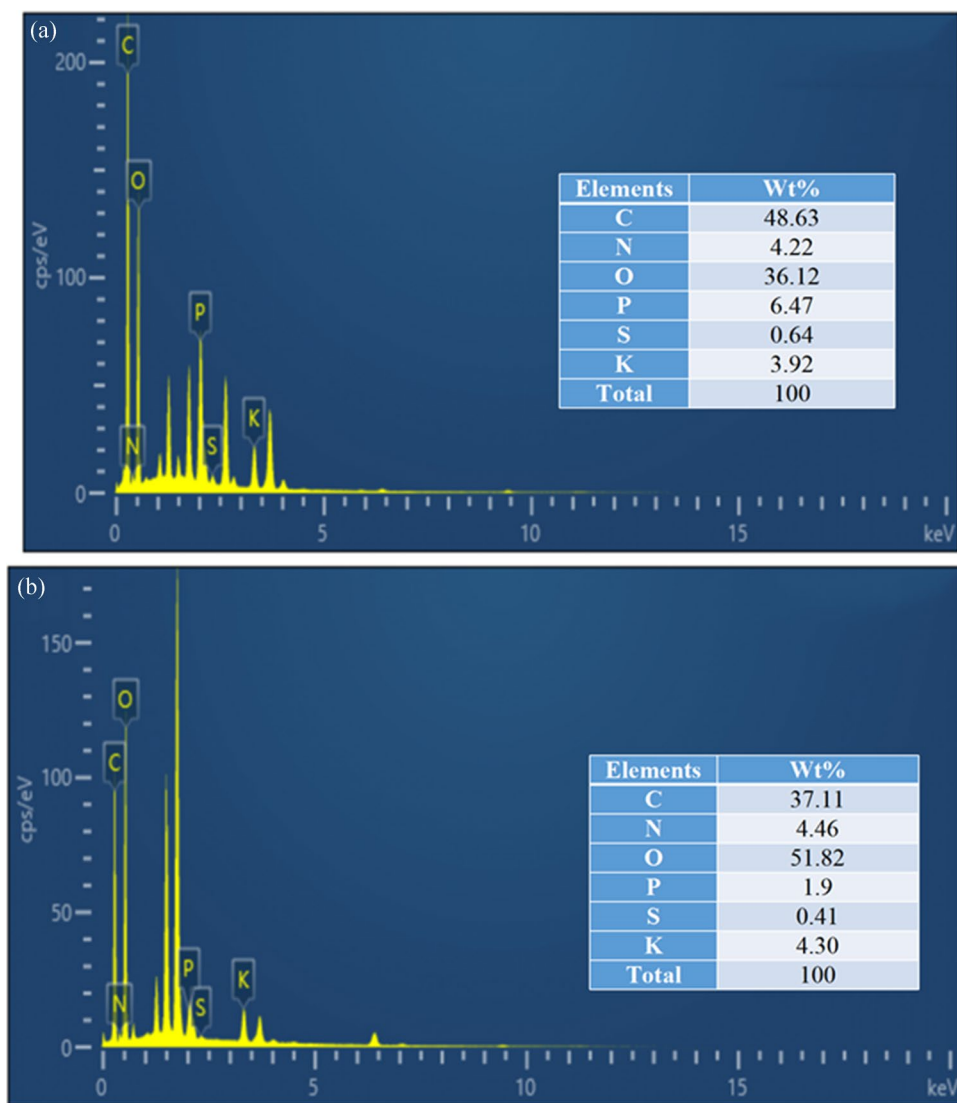


Table 1 Elemental analyzer results and zeta potential of the prepared materials

Materials	N/%	C/%	H/%	S/%	Zeta potential/mV
MB	0.577	55.900	6.223	0.532	-22.0
NMB	3.585	52.425	3.014	0.078	-24.3

the mask polymer (polyester fibers), and may be influenced by the nitrogen-containing dyes in the waste masks (Luo et al. 2021; Oginni 2022). Moreover, MB₀, MB, and NMB contained similar FTIR characteristic spectra near 700–878 cm⁻¹ searched in the spectral database (<http://www.sciencedirect.com/science/article/pii/S0926641022000000>), which may be the characteristic peaks of ketone or ester compounds (Emenike et al. 2022). This not only indirectly confirms the N modification into NMB, but also suggests that the use of waste masks enriches the functional group types on the biochar surface. With the

introduction of nitrogen, the species of NMB surface functional groups remained unchanged relative to the MB; however, the functional group levels increased slightly, especially at -OH, -COOH, and heterocyclic functional groups. This implies that nitrogen modification enhances the surface functional group concentration, which may be attributed to the activation of N (Brillard et al. 2021).

BET surface area and pore size analysis

The specific surface area characteristics of the prepared materials are shown in Table 2 and Fig. 5. According to the International Union of Pure and Applied Chemistry (IUPAC), it could be found that CB, MB, and NMB are mesoporous materials attributed to their average pore size ranging from 2 to 50 nm (Wang et al. 2021b). It could be attributed to the experimental conditions as pyrolysis was performed at 450 °C and a rate of 5 °C·min⁻¹ (Wang and

Fig. 4 XRD and FTIR analysis of the prepared materials: **a** for XRD, **b** for FTIR

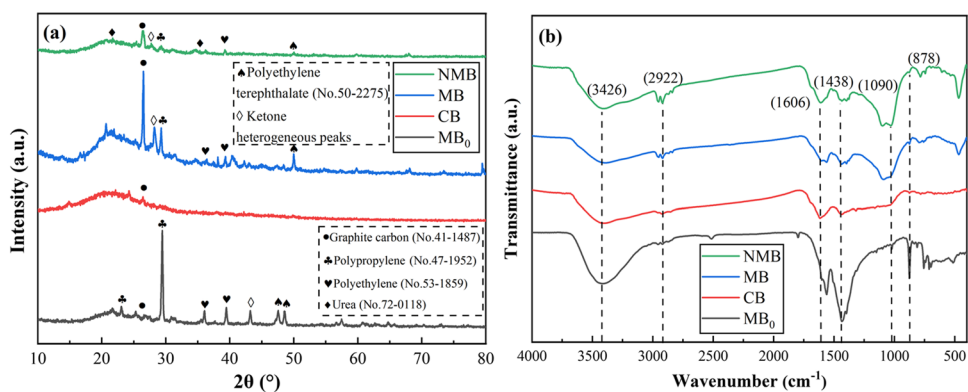
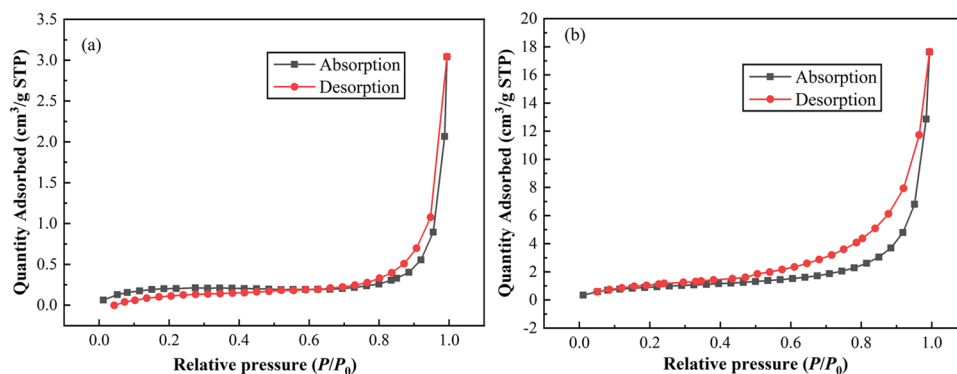


Table 2 Specific surface area and pore size distribution characteristics of the prepared materials

Materials	Langmuir-specific surface area $S_L/m^2 \cdot g^{-1}$	BET-specific surface area $S_{BET}/m^2 \cdot g^{-1}$	Pore volume/ $cm^3 \cdot g^{-1}$	Pore size/nm
MB ₀	- ¹	-	-	-
CB	10.62	1.42	0.01	16.21
MB	29.37	2.35	0.02	31.33
NMB	63.10	3.35	0.03	32.33

¹“-” means have not been detected or not determined

Fig. 5 Adsorption–desorption isotherms for the prepared materials: **a** for MB, **b** for NMB



Husein 2023). Emissions of pyrolysis gases could help in cavity formations and production of mesoporous materials, which usually have abundant porous structures and contribute to good adsorption performance (Tang et al. 2022). Figure 5 illustrates that both MB and NMB belong to type IV isotherms and are accompanied by obvious hysteresis loops, which also confirms that the materials are mesoporous (Bi et al. 2020). Probably due to factors such as incomplete N modification (Qiang et al. 2023), there is adsorption and desorption separation of MB at low relative pressures. However, this may also be influenced by the pyrolysis feedstock being a polymer such as polypropylene (Yuwen et al. 2022). Moreover, the data in Table 2 could reflect the phenomenon, that is, MB₀ is not a porous material. Since MB₀ may not contain a porous structure causing the relevant data not to be detected, which is mutually confirmed by the FESEM

images in Fig. 2a. Furthermore, the data in Table 2 also indicated that nitrogen modification significantly increased the specific surface area and pore volume of the biochar. Moreover, the MB prepared by co-pyrolysis also showed an increase in specific surface area and pore volume over the CB prepared from a single feedstock.

Zeta potential and contact angle analysis

As shown in Table 1, the zeta potentials of MB and NMB are −22.0 and −24.3 mV at room temperature conditions, respectively. This suggests that both surfaces may be negatively charged, with the NMB being more highly charged. The contact angle of the NMB is shown in Fig. S1 (Supplementary Material). With 20 kN compression, the droplet just contacted the surface of NMB first penetrated slowly and

then stabilized. The contact angle of NMB was determined as 82.3° , which means that NMB is hydrophilic ($<90^\circ$). This also implies the possibility of these adsorbents being applied to aqueous environments.

Adsorption characteristics

In this work, the adsorption characteristics of NMB were evaluated by three aspects: comparison of adsorption capacity, isotherms adsorption, and adsorption kinetics.

Comparison of adsorption capacity before and after nitrogen modification

The comparison of the adsorption capacity of BPA by the materials is shown in Fig. 6. It is observed that with the increase of adsorption time, the adsorption of BPA by the four materials gradually increased until the adsorption equilibrium was reached. Particularly, the average adsorption capacity of BPA by NMB was the largest, followed by MB, CB, and MB_0 . In terms of the maximum adsorption capacity, the adsorption of BPA by NMB was 2.35, 3.53, and 5.58 times higher than that of MB, CB, and MB_0 , respectively. It is evident that the NMB has certain advantages and potentially indicates the possibility of waste mask utilization. Additionally, it could be observed from Fig. 6 that the adsorption of BPA by MB_0 is very small and reaches adsorption equilibrium in a shorter time, which could be attributed to the nonporous. CB and MB gradually reached adsorption equilibrium only at 12 h, while NMB demanded 24 h. This is likely attributed to the activating effect of nitrogen modification on the surface properties of the biochar, together with

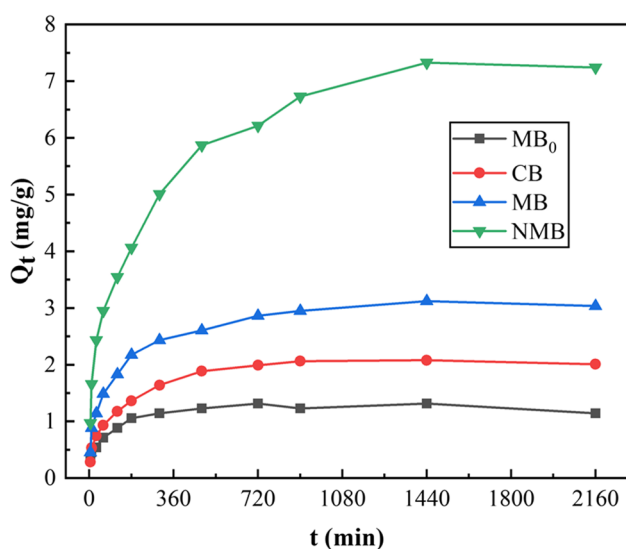


Fig. 6 Comparison of BPA adsorption by the prepared materials

the waste masks enriching the surface functional groups and shaping the microsphere structure (Wang et al. 2021a).

Isotherm adsorption

Figure 7 shows the fitted curve of isothermal adsorption of BPA on NMB, indicating that the adsorption capacity gradually increased with the increase of the initial concentration of BPA. Specifically, when the initial concentration of BPA was in the range of $1\text{--}50\text{ mg}\cdot\text{L}^{-1}$, the equilibrium concentration was in the range of $0.48\text{--}20.66\text{ mg}\cdot\text{L}^{-1}$. The fitted adsorption isotherms were very steep, implying that the adsorption capacity of BPA on NMB increased linearly and rapidly from 0.52 to $29.34\text{ mg}\cdot\text{g}^{-1}$. When the initial concentration of BPA was between 100 and $300\text{ mg}\cdot\text{L}^{-1}$, the equilibrium concentration of BPA increased from 61.94 to $237.37\text{ mg}\cdot\text{L}^{-1}$. However, the adsorption capacity increased slowly from 38.06 to $62.63\text{ mg}\cdot\text{g}^{-1}$, which gradually stabilized and reached the adsorption equilibrium. The overall trend of the adsorption isotherms is first fast, then slow, and finally smooth, which is attributed to the gradual occupation of the adsorption sites in the NMB by BPA until saturation (Wang et al. 2017).

The isothermal adsorption model fitting parameters are shown in Table 3. The Langmuir, Freundlich, and Temkin models all have a goodness-of-fit (R^2) greater than 0.95, which is significantly higher than that of the D-R model. However, the R^2 of the Temkin model was slightly larger than that of the Langmuir and Freundlich models, implying that the adsorption process is complicated and may include chemisorption besides the physical process (Wang et al. 2021a). The theoretical maximum adsorption of BPA by NMB was calculated to be $61.81\text{ mg}\cdot\text{g}^{-1}$ from the Langmuir

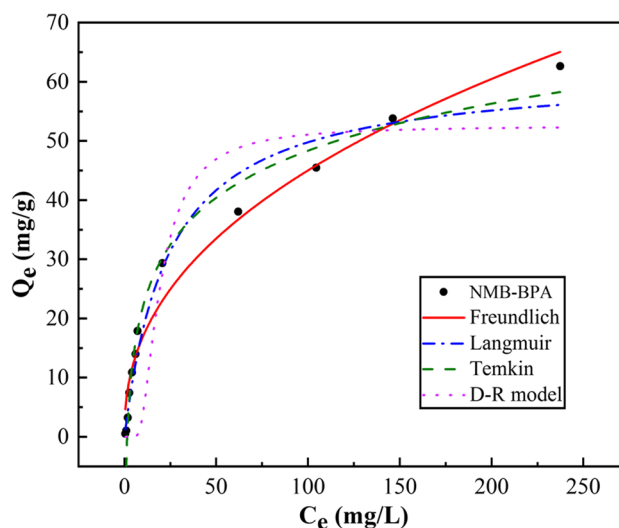


Fig. 7 Isotherm adsorption of BPA by NMB

Table 3 Isothermal adsorption fitting parameters of BPA by NMB

Material	Langmuir			Freundlich			Temkin			D-R model		
	<i>a</i>	$Q_m/\text{mg}\cdot\text{g}^{-1}$	R^2	K_F	<i>n</i>	R^2	<i>A</i>	<i>B</i>	R^2	$Q_0/\text{mmol}\cdot\text{g}^{-1}$	$E/\text{kJ}\cdot\text{mol}^{-1}$	R^2
NMB	0.0413	61.806	0.971	6.329	2.347	0.972	0.677	11.472	0.980	52.536	0.104	0.875

model, which is basically similar to the experimental data of $62.63 \text{ mg}\cdot\text{g}^{-1}$. This also indicates that the adsorption process may be explained by the Langmuir model, i.e., monomolecular layer adsorption. From the values of parameter *a* in Table 3 and the initial concentration c_0 , the R_L is calculated to be 0.07–0.96, which belongs to the range of 0–1, indicating that the adsorption process of BPA by NMB is beneficial adsorption (Qiang et al. 2023). Additionally, in the Freundlich model, *n* is equal to 2.347, which is greater than 2, indicating that the adsorption strength of BPA is high (Tang et al. 2022). In the D-R model, the adsorption energy *E* of BPA by NMB was $0.104 \text{ kJ}\cdot\text{mol}^{-1}$, indicating that the adsorption process of BPA on NMB might be dominated via physical action (Wang et al. 2021b). Q_0 was the unit maximum adsorption capacity of $52.536 \text{ mmol}\cdot\text{g}^{-1}$, which was lower than the theoretical and experimental maximum adsorption capacity.

Adsorption kinetics

Figure 8 shows the fitting curve of the adsorption kinetics for BPA on NMB. It is shown that the adsorption capacity of BPA increased gradually with the increase of adsorption time. The adsorption trend was “first fast and then slow” (Li et al. 2023b), and reached the adsorption equilibrium at 24 h. Specifically, NMB adsorbed BPA faster at 3 h, about 56% of maximum adsorption capacity. The adsorption time at 3–24 h was more stable and the adsorbed amount increased slowly. When the adsorption time reached 36 h, the desorption phenomenon occurred. This is inextricably linked to the saturated adsorption sites and decreased adsorption rates (Wang et al. 2021a; Shi et al. 2022).

As shown in Table 4, the pseudo-second-order (using a linear transformation) and Elovich model have higher R^2 than other models. Especially, the pseudo-second-order is the most suitable model with an adsorption rate constant of $1.065 \text{ g}\cdot\text{mg}^{-1}\cdot\text{min}^{-1}$. Moreover, the pseudo-second-order kinetic model fitted a maximum adsorption capacity of $7.021 \text{ mg}\cdot\text{g}^{-1}$, which is closer to the experimental result than the pseudo-first-order. The pseudo-second-order kinetic model could comprehensively describe the adsorption process, including the processes of external liquid film diffusion, surface adsorption, and intraparticle diffusion (Wang et al. 2017). It means that the adsorption process could be considered to contain both physical and chemical adsorption, which is a more true reflection of the adsorption mechanisms of

BPA by NMB. Comparatively, the R^2 of the Elovich model is also higher indicating that the NMB has a uniformly distributed surface adsorption energy (Tang et al. 2022), which is affected by N activation and the special structure of the NMB, where the desorption constant *b* is greater than the adsorption constant *a*, indicating that the adsorption of NMB on BPA is not stable and is prone to desorption (Shi et al. 2022). The fitting results of the intraparticle diffusion model showed that particle diffusion is not the only rate-limiting factor (Wang et al. 2021b). The surface adsorption and liquid film diffusion are also involved in controlling the adsorption rate of BPA in combination with the optimal model. Moreover, the coefficient *C* was 1.763 in intraparticle diffusion model, indicating that the NMB boundary layer has some influence on the adsorption of BPA (Li et al. 2023b).

Adsorption mechanisms

Exploring the adsorption mechanisms of BPA on NMB could help promote its popularization in practical environmental applications, and also provide new ideas for the design of new mask-based biochar. Based on the above analysis results, it could be deduced that the adsorption processes of BPA onto NMB include both physisorption and chemisorption (Wang et al. 2021b). Combining the optimal kinetic adsorption model, the physical adsorption of BPA by NMB includes liquid film diffusion, surface adsorption, and intraparticle diffusion (Li et al. 2023b). Therein, the liquid film diffusion is mainly caused by the concentration difference of the solvent BPA. So, surface diffusion and intraparticle diffusion are the most dominant physical adsorption processes (Qiang et al. 2023). Surface diffusion may be related to the van der Waals force between the solute BPA and the adsorbent NMB (Brillard et al. 2021). Intraparticle diffusion is mainly attributed to the mesoporous structure and surface properties of NMB (Tang et al. 2022).

To further investigate the chemical effect, the NMB samples before and after adsorption of BPA were separated, dried, and analyzed using FTIR and XPS, as shown in Fig. 9. It is observed that the phenolic hydroxyl group stretching vibration peak at 3420 cm^{-1} of NMB is significantly weakened after adsorption (Fig. 9a). This indicates that the phenolic hydroxyl groups on the NMB surface may be bound or masked during the adsorption process because the BPA surface also contains less –OH. If the complexation reaction occurs, a lot of BPA occupies the active sites on the

Fig. 8 Adsorption kinetics of BPA by NMB. **a** Three adsorption kinetic models, **b** pseudo-second-order (using a linear transformation)

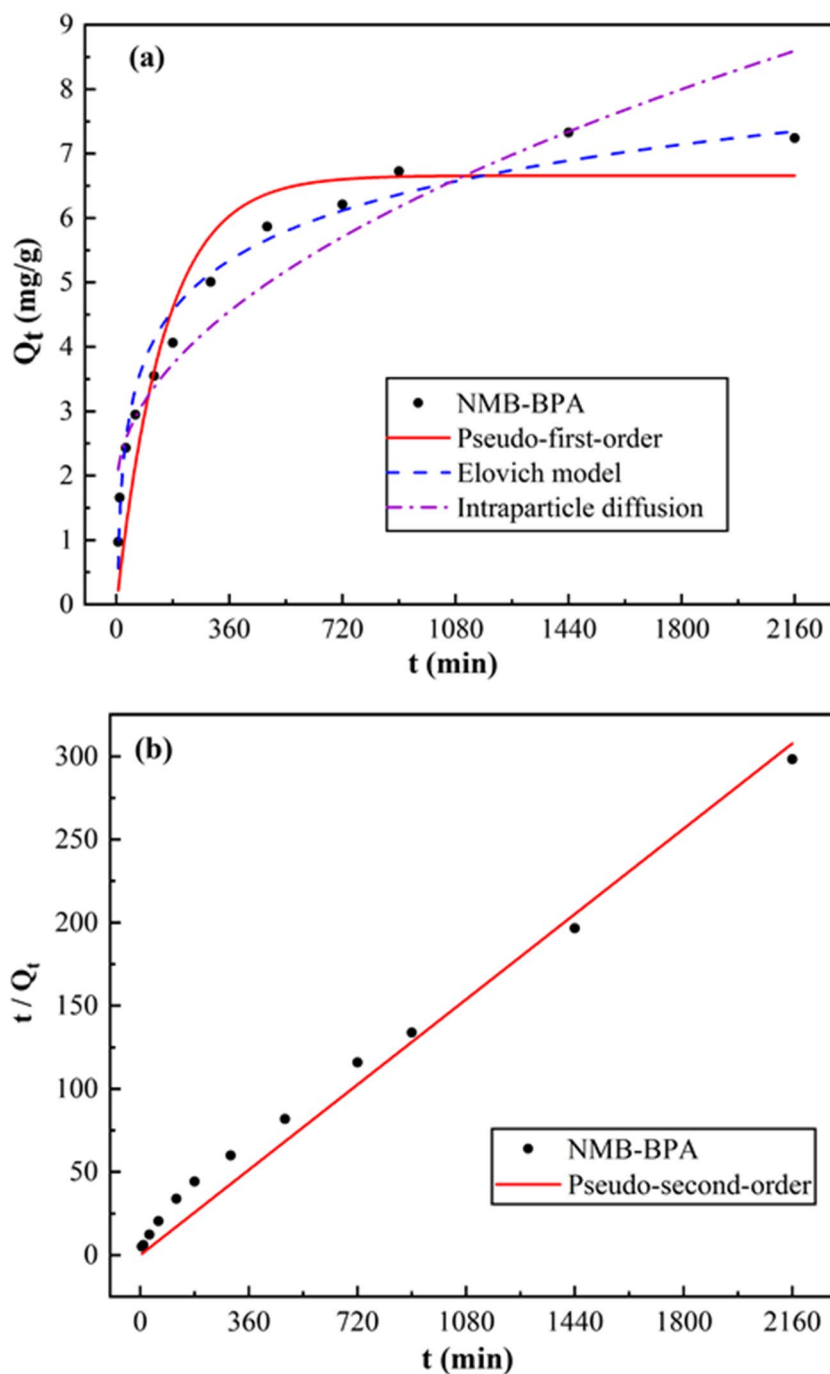


Table 4 Adsorption kinetics fitting parameters of BPA by NMB

Material	Pseudo-first-order			Pseudo-second-order			Elovich			Intraparticle diffusion		
	$Q_e/\text{mg}\cdot\text{g}^{-1}$	k_1	R^2	$Q_e/\text{mg}\cdot\text{g}^{-1}$	k_2	R^2	a	b	R^2	k_i	C	R^2
NMB	6.6595	0.015	0.871	7.021	1.065	0.978	0.369	0.895	0.971	0.147	1.763	0.889

NMB surface, resulting in the shielding of the NMB surface. Thus, the characteristic peaks of $-\text{OH}$ here after adsorption of BPA are significantly weakened. The molecular hydrogen

bonding force of intramolecular $-\text{OH}$ is weakened because phenolic hydroxyl groups are often covalently bonded on adsorbents and are not ions. Hence, phenolic hydroxyl

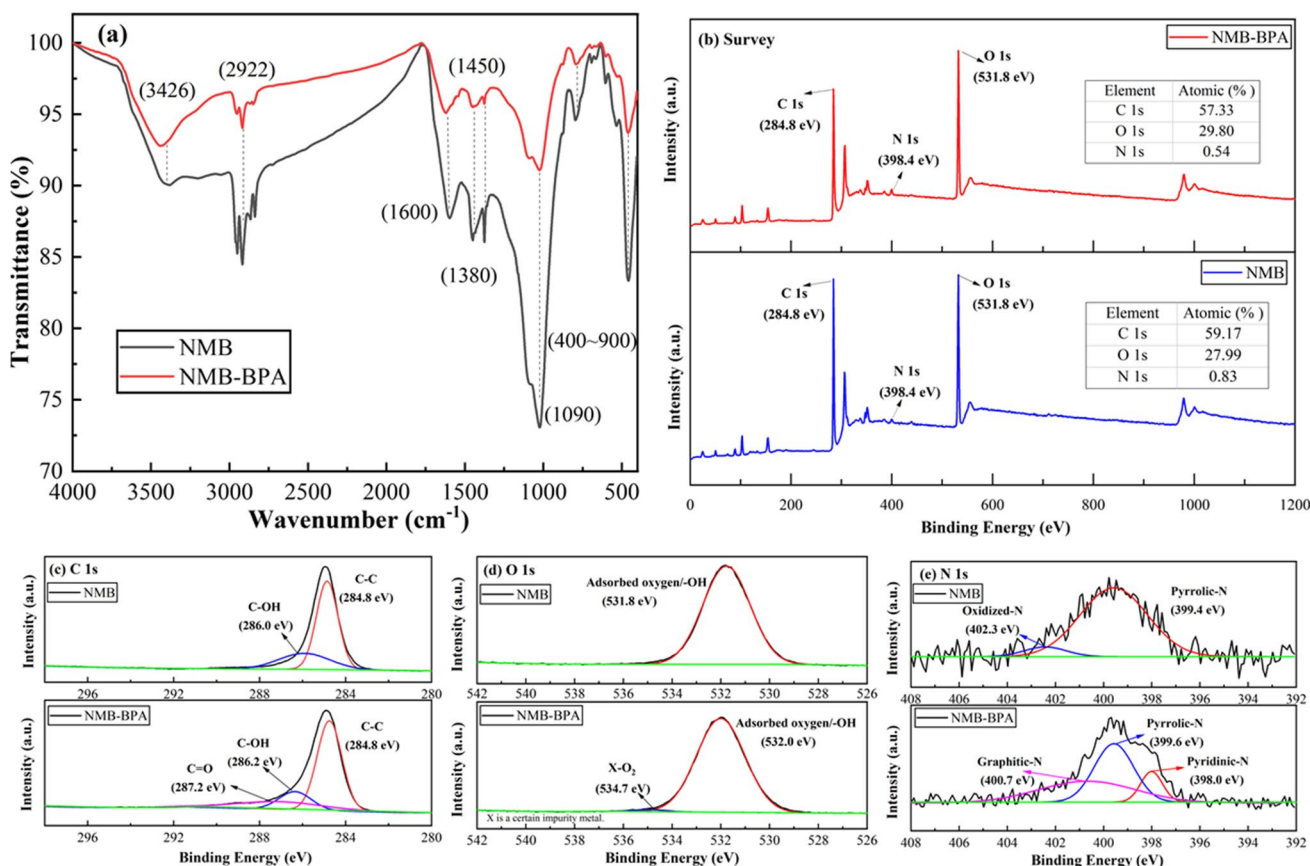


Fig. 9 FTIR and XPS spectra of BPA before and after BPA adsorption by NMB. **a** FTIR, **b** survey, **c** C 1s, **d** O 1s, and **e** N 1s

exchange is generally considered to be a ligand-exchange process, which implies that ligand-exchange action occurs during the adsorption of BPA by NMB (Wang et al. 2017; Ye et al. 2020). Similarly, the amino vibrational peaks ($-\text{NH}_2$) near 1600 cm^{-1} and the aromatic acidic vibrational peaks ($-\text{COOH}$) near 1437 cm^{-1} were also significantly weakened by the adsorption of BPA, implying the presence of ion exchange. Moreover, BPA is usually hydrolyzed to negatively charged groups in acidic and alkaline solutions (e.g., Fig. 10). Also, the amino group may dissociate H^+ to undergo charge attraction with BPA (Song et al. 2020). Of course, it is also possible to deduce that the above phenolic hydroxyl group, $-\text{COOH}$, and the negatively charged BPA group may also be hydrogen bonded, a weak intermolecular force. Moreover, the C–C or C=C peaks of NMB at 1380 cm^{-1} and 1090 cm^{-1} were significantly weakened after the adsorption of BPA, especially at 1090 cm^{-1} , which implies the presence of π – π interaction. This is attributed to the conjugation vibration of the C=C/C–C bond and the nitrogen-containing functional groups with the benzene ring of BPA during adsorption, resulting in a decrease in the relative levels (Qiang et al. 2023). Furthermore, the aromatic compounds and ester heterocyclic functional groups at 400 – 900

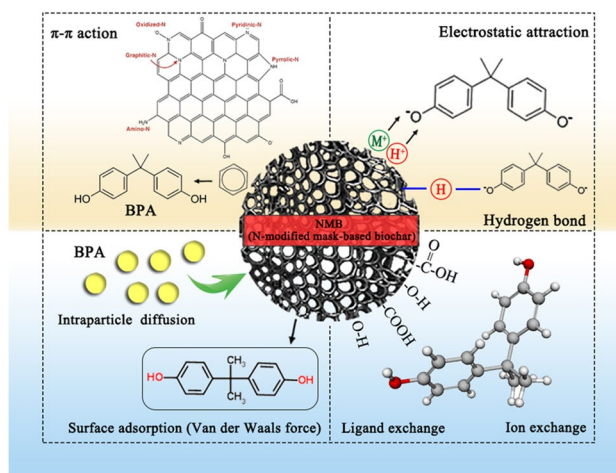


Fig. 10 Adsorption mechanisms of BPA on NMB

cm^{-1} were also significantly weakened upon adsorption of BPA, which may still be attribute to π – π bond interactions (Tang et al. 2022).

Figure 9b shows that the C and N element contents on the NMB surface decreased and the O element content increased

after adsorption of BPA. This indicates that the bond-valent structure of these elements was involved in the adsorption process of BPA, but the overall content change was not significant. Figure 9c illustrates that the C–C bond of the C carbon skeleton at 284.8 eV is essentially unchanged. However, the energy of the C–OH bond at 286.0 eV is slightly raised, which confirms laterally that ligand exchange and ion exchange associated with –OH exist in the adsorption process (Qiang et al. 2023). Moreover, the C=O bond at 286.0 eV was also fitted after the adsorption of BPA, which may suggest the presence of π – π bonding interactions (Li et al. 2023b). These analyses are in agreement with the FTIR results. Furthermore, the O 1s spectra of Fig. 9d illustrate that the adsorbed oxygen –OH at 531.8 eV increases in energy to 532.0 eV with the adsorption of BPA. And this shift in the high-energy spectra implies the involvement of –OH in the adsorption process (Wang et al. 2021b). Surprisingly, a weak X–O₂ bond was also found at 534.7 eV. This is attributed to the presence of minor heavy metal impurities in the cow dung, which are positively charged and bind to the negatively charged BPA in solution (Wang and Husein 2023). This confirms the existence of electrostatic attraction. Moreover, Fig. 9e demonstrates the changes of N 1s after the adsorption of BPA, indicating that NMB contains a small percentage of oxidized nitrogen (402.3 eV). This may be related to the oxidation of nitrogen-containing dyes and polyester fibers in the waste masks during high-temperature pyrolysis or high-pressure hydrothermal reaction. The disappearance of nitrogen oxide at 402.3 eV after adsorption of BPA suggests that nitrogen oxides originally in the NMB are conjugated (e.g., complexation reaction) with BPA and thus converted to other nitrogen. This led to the detection of pyridine nitrogen (398.0 eV) and graphite nitrogen (400.7 eV) after adsorption of BPA, which may be related to π – π bond conjugation (Qiang et al. 2023). Additionally, the binding energy of pyrrole nitrogen (399.4 eV) was elevated to 399.6 eV after the adsorption of BPA, which side-by-side reflected that nitrogen activated the surface structure and participated in the adsorption reaction (Li et al. 2023b). This might be related to the occurrence of π – π bonding conjugation between heterocyclic functional groups and the benzene ring of BPA (Choi and Kan 2019; Jia et al. 2019).

Additionally, a review of related literature found that BPA adsorption by biochar is associated with weak intermolecular forces of electron transfer and hydrophobic interactions of the Lewis acid base theory (Zhang et al. 2020). Both effects may exist in depth, but further exploration is needed to verify this. According to the Lewis acid base theory and the characterization data (Fig. 9), ion or ligand exchange occurs with electron/charge transfer (Wang and Husein 2023). In turn, hydrophobic interactions may also be related to the hydrogen bonding between solvent and solute discussed above. Consequently, the main adsorption

mechanisms of BPA on NMB are a combination of physical and chemical adsorption, including π – π interaction, electrostatic attraction, hydrogen bonding, intraparticle diffusion, surface adsorption, and ion or ligand exchange. In particular, quantitative analysis showed that π – π action and hydrogen bonding may be the main contributions. These adsorption mechanisms are summarized as shown in Fig. 10, which is mainly attributed to the mesoporous structure, surface properties, abundant surface functional groups, and nitrogen-modified (Lu et al. 2017; Baldikova et al. 2020). The fundamental reason for this is closely related to the co-pyrolysis of waste masks and cow dung biomass selected for this study, which was also influenced by nitrogen modification.

Adsorption capacity of BPA on biochar prepared from different feedstocks

Table 5 summarizes the reports related to the adsorption of BPA by various biochar. Under similar experimental conditions, a comparison of these data reveals that the maximum adsorption of BPA by NMB in this work was significantly higher than that of biochar prepared from some raw materials, such as bamboo-based biochar, cypress twig biochar, marine alga *U. prolifera* biochar, and rice husk biochar. It also has better adsorption properties than some modified biochar, including potassium carbonate–modified reed biochar. Meanwhile, there was little difference in the adsorption of BPA between NMB and alfalfa biochar and magnetic iron oxide–modified biochar. This indicates that the NMB prepared from waste masks still has advantages in the adsorption of BPA compared to biochar prepared from conventional biomass or even modified biochar (Mpatani et al. 2021; Qu et al. 2020). After all, the co-pyrolysis of waste masks prepared as composite carbon materials and the exploration of emerging pollutants removal from water bodies already have methodological novelty. Additionally, Table 5 reflects that the adsorption of BPA by NMB was significantly lower than some modified biochars, such as phosphoric acid–modified biochar, expanded activated biochar, and KOH-activated reed biochar. This is related to the modification method, material structure, and physicochemical properties. It also reflects the upper limit of mask-based biochar, and the adsorption performance is not outstanding. However, on balance, NMB showed a higher adsorption capacity for BPA and a relatively shorter adsorption time, and it was able to meet the practical applications for domestic or industrial wastewater (Mpatani et al. 2021). If the resourceization of waste masks and indirectly solving the disinfection treatment of pathogens are considered, the co-pyrolysis and the modification methods proposed in this study have potential promotion prospects.

Regarding the best isothermal adsorption model, most of them are Freundlich, which assumes an inhomogeneous

Table 5 Comparison of the adsorption capacity of biochar derived from different materials

Biochar types	Maximum adsorption capacity ¹ (mg·g ⁻¹)	Literature	Optimal isotherm model	Optimal kinetic model
Bamboo-based biochar	2.75	Zhang et al. 2023	Freundlich	Pseudo-second-order
Potassium carbonate-modified reed biochar L55C	28.55	Pan et al. 2022	Langmuir	Pseudo-second-order
Phosphoric acid-modified biochar	250.00	Ye et al. 2020	Freundlich	Pseudo-second-order
KOH-activated reed biochar 650K3	145.84	Song et al. 2020	Freundlich	Pseudo-second-order
Expanded-activated biochar HC	220.74	Xu et al. 2023	Langmuir	Pseudo-second-order
Cypress branch biochar BC700	57.00	Jia et al. 2019	Freundlich	Pseudo-second-order
Alfalfa biochar AF650	62.70	Choi and Kan 2019	Temkin/Langmuir	Pseudo-second-order
Marine algae <i>U. prolifera</i> biochar	33.30	Lu et al. 2017	Langmuir	Pseudo-second-order
Magnetic iron oxide-modified biochar	77.40	Baldikova et al. 2020 - ²		Pseudo-second-order
Rice husk biochar	56.61	Qu et al. 2020	Freundlich	Pseudo-second-order
NMB	62.63	This work	Temkin	Pseudo-second-order

¹The maximum adsorption capacity in this table is the maximum value both of the actual adsorption capacity and theoretical maximum adsorption capacity calculated by the Langmuir model under aqueous solution conditions

²Lack of relevant data

adsorption surface and adsorption heat (Wang et al. 2021b). The Freundlich model describes the adsorption behavior of highly heterogeneous adsorbents, so it is commonly used for adsorption processes in composites with non-monomolecular layers. The best isothermal adsorption model for NMB is Temkin, which is supported by the study of Choi and Kan (2019). Moreover, the Freundlich model in this study also had a high R^2 , which laterally explains the adsorption process of BPA by the composite NMB; therefore, this difference may be almost ignored. Regarding the optimal adsorption kinetic model, only the literature reported in Table 5 is pseudo-second-order models, which is attributed to an integrated complex adsorption process. It assumes that the rate of adsorption is controlled by a chemisorption mechanism involving electron transfer between adsorbent and adsorbate (Qiang et al. 2023).

Discussion of environmental risks

Furthermore, many studies lacked environmental risk evaluation for the application of new eco-friendly materials (Mpatani et al. 2021), which is also a “sensitive point” of interest to readers. This study briefly explores the potential for the release of secondary pollutants from the prepared materials in the aqueous environment based on the organic leaching tests. XRD and FTIR characterization data (Fig. 4) indicated that MB₀, MB, and NMB surfaces may contain substances such as polypropylene, polyethylene, polyethylene terephthalate, and the corresponding functional groups. So, could these substances be leached causing a risk of secondary pollution? This is a very interesting topic. However, the GC–MS data from the leaching tests showed that

polypropylene, polyethylene, and polyethylene terephthalate were not detected in the leachates of MB₀, MB, and NMB. It is mainly attributed to the high temperature carbonization of waste masks by co-pyrolysis and hydrothermal synthesis is a relatively stable thermal reaction, which may immobilize crystals of the abovementioned risky substances into the materials or form the functional groups (Luo et al. 2021; Emenike et al. 2022). This also implies the possible green nature of preparing carbon materials from waste masks as a carbon source. Although the above substances were not detected, the environmental risk of NMB in water treatment applications still needs to be carefully evaluated by more tests (Brillard et al. 2021). As such, NMB has the potential for safe applications.

Cost estimates and prospects

The cost required for the preparation of NMB was estimated using the life cycle assessment method (Wang et al. 2021a) in Table 6. In the scenario simulation, the main considerations are the cost of raw materials, manual collection, transportation, electricity consumption (pyrolysis, hydrothermal reaction, dry, and energy loss), and other cost. The total cost of preparing 1 kg of NMB is estimated to be approximately 27.76 USD. If only the cost of the preparation process (i.e., electricity) is taken into account, the cost of producing 1 kg of NMB is approximately 7.21 USD. It is difficult to obtain complete statistics on the productivity and costs of this process in different countries or regions worldwide; moreover, many factors affect the cost. Therefore, the production costs of NMB were evaluated based on the production data in China, and the

Table 6 Estimation of the cost required to prepare 1 kg of NMB by life cycle evaluation method

Scenario ¹	Unit price ²	Quantity and units ³	The cost of producing 1 kg NMB	Description
Waste masks	¥ 0.00/kg ⁴	3 kg	¥ 0.00	As waste, the cost is ignored
Biomass (cow dung)	¥ 0.00/kg	3 kg	¥ 0.00	As waste, the cost is ignored
Manual collection	¥ 120.00	1 person per day	¥ 120.00	It takes one person to collect 6 kg of raw materials in 1 day
Transportation cost	¥ 30.00	6 kg, 150 km	¥ 30.00	Logistics price, the distance not more than 150 km around the city
Pyrolysis cost	¥ 0.50 (electricity price, 1 kW·h)	3 h, P= 10 kW (industrial furnace)	¥ 15.00	According to relevant reports (Wang et al. 2021a), the yield of biochar is about 30% of the total biomass, using a large industrial furnace to prepare. The volume of the industrial furnace is 1 m ³ and the power (P) is 10 kW
Urea	¥ 2.20/kg	0.3 kg	¥ 0.66	According to the mixing ratio, about 0.3 kg of urea is required as the N-modified precursor. Using CME international futures prices for urea in May 2024
Hydrothermal reaction and dry	¥ 0.50 (electricity price, 1 kW·h)	P=2 kW, the hydrothermal reaction takes 10 h and drying for 10 h	¥ 20.00	Using industrial reactors and drying equipment. The power (P) is 2 kW
Energy loss	¥ 0.50 (electricity price, 1 kW·h)	1 h, P= 10 kW; 2 h, P=2 kW	¥ 7.00	The main consideration is the power loss during pyrolysis and hydrothermal reaction
Other	-	1 kg NMB	¥ 10.00	Considering the additional cost of N ₂ , manual filling of material, pick-up, etc
Total	-	-	¥ 202.66	Sum the above. If only the cost of the preparation process is considered, it costs ¥ 52.66 to product 1 kg of NMB
Exchange rate conversion	-	-	\$ 27.76	Using an average exchange rate of 7.3 for May 2024. If only the cost of the preparation process (i.e., electricity) is considered, it costs \$ 7.21 to product 1 kg of NMB

¹The scenario in the table refers to related research reports (Wang et al. 2021a)

²The “Unit price” data comes from the average value estimated by the IPCC Comprehensive Assessment Report (2014) and the Yearbook of the National Bureau of Statistics of China. In particular, the data for electricity prices are from the U.S. Industrial Electricity Prices

³The “Quantity and units” data comes from actual simulation situations and related industrial equipment

⁴¥ denotes the Chinese Yuan (CNY), and \$ denotes the United States dollar (USD)

international currency US dollar is used as the final settlement here (Wang et al. 2021a). Taken together, this treatment cost is likely to be lower than the cost of treating waste masks and waste biomass separately (Yuwen et al., 2021a), thereby hinting at the green concept of “turning waste into treasure.” Additionally, the research on NMB in actual wastewater treatment and soil column simulation

experiments is still worth exploring. The adsorption thermodynamics, the effect of interfering ions, the desorption case, and the reusability need to be further explored in this process as well (Al-sareji et al. 2024a; b). In conclusion, this study gives us reason to believe that waste masks and biomass could be prepared as adsorbents with good performance via co-pyrolysis.

Conclusion

In this study, waste masks were used as raw materials to prepare mask-based biochar by a novel method of copyrolysis with cow dung biomass. Urea was introduced as a nitrogen modification reagent to prepare NMB via hydrothermal synthesis. Several characterizations revealed that the waste masks are involved in thermochemical reactions and shape the microsphere structure of the biochar, which enhances the types of surface functional groups, especially ester groups and aromatic heterocycles. Nitrogen modification enriches the surface elemental composition and activates the specific surface area, which in turn enhances the adsorption performance. The average adsorption capacity of BPA on NMB was the largest, which was 2.35–5.58 times higher than that of the three control materials. Temkin model and pseudo-second-order could well describe the isothermal and kinetic adsorption process of BPA on NMB. The adsorption process was mainly physicochemical composite adsorption. The experimental maximum adsorption capacity of BPA by NMB was 62.63 mg·g⁻¹, and the adsorption equilibrium was reached within 24 h. The adsorption rate constant was 1.065 g·mg⁻¹·min⁻¹. The adsorption process of BPA by NMB was characterized by a combination of physical and chemical adsorption, and the adsorption mechanisms were mainly dominated by π - π interaction, electrostatic attraction, hydrogen bonding, intraparticle diffusion, surface adsorption, and ionic or ligand exchange, as analyzed by FTIR and XPS. The GC-MS data from the leaching tests showed that polypropylene, polyethylene, and polyethylene terephthalate were not detected in the leachates of the prepared adsorbents. After assessment, the total cost of preparation of NMB is about 27.76 USD per kg, with a cost of 7.21 USD per kg for the preparation process alone. The methodology and composite design of this study are novel, and the large adsorption of BPA suggests that NMB has some potential for application.

Supplementary Information The online version contains supplementary material available at <https://doi.org/10.1007/s11356-024-34605-y>.

Author contribution Tongtong Wang: conceptualization, visualization, formal analysis, methodology, funding acquisition, project administration, writing—original draft. Dalal Z. Husein: writing—review and editing. Siyan Guo, Xinle Zhang, Jiarui Kang, Huixia Wang, and Shumiao Cao: data curation, investigation, validation. Zhonghua Shanguan: resources, validation. Hui Shi: resources, supervision, funding acquisition, project administration, writing—review and editing.

Funding This work was funded by the Key Research and Development Program of Shaanxi Province (No. 2023-LL-QY-42; 2024NC-ZDCYL-02-05), the Xi'an University of Architecture and Technology Research Initiation Grant Program (No. 1960323102), and the Xi'an University of Architecture and Technology Special Program for Cultivation of Frontier Interdisciplinary Fields (No. X20230079).

Data availability The datasets used during the current study are available from the corresponding author on reasonable request.

Declarations

Ethics approval Not applicable.

Consent to participate Not applicable.

Consent to publish The authors confirm that the final version of the manuscript has been reviewed, approved, and consented for publication by all authors.

Competing interests The authors declare no competing interests.

References

- Al-sareji OJ, Al-Samarrai SY, Grmasha RA, Meiczinger M, Al-Juboori RA, Jakab M, Somogyi V, Miskolczi N, Hashim KS (2024a) A novel and sustainable composite of L@PSAC for superior removal of pharmaceuticals from different water matrices: production, characterization, and application. *Environ Res* 251:118565
- Al-sareji OJ, Grmasha RA, Meiczinger M, Al-Juboori RA, Somogyi V, Hashim KS (2024b) A Sustainable banana peel activated carbon for removing pharmaceutical pollutants from different waters: production, characterization, and application. *Materials* 17:1032
- Baldikova E, Pospiskova K, Safarik I (2020) Removal of bisphenol A using magnetically responsive spruce chip biochar. *Chem Eng Technol* 43(1):168–171
- Bi WW, Chen Y, Ma XY, Deng Q (2020) Synthesis of magnetic ordered mesoporous carbon and its adsorption of bisphenol A in water. *China Environ Sci* 40(11):4762–4769
- Brillard A, Kehrli D, Douguet O, Gautier K, Tschamber V, Bueno MA, Brillhac JF (2021) Pyrolysis and combustion of community masks: thermogravimetric analyses, characterizations, gaseous emissions, and kinetic modeling. *Fuel* 306:121644
- Choi YK, Kan E (2019) Effects of pyrolysis temperature on the physicochemical properties of alfalfa-derived biochar for the adsorption of bisphenol A and sulfamethoxazole in water. *Chemosphere* 218:741–748
- Desai AN, Aronoff DM (2020) Masks and coronavirus disease 2019 (COVID-19). *JAMA, J Am Med Assoc* 323(20):2103
- Emenike EC, Iwuozor KO, Agbana SA, Otoikhian KS, Adeniyi AG (2022) Efficient recycling of disposable face masks via co-carbonization with waste biomass: a pathway to a cleaner environment. *Cleaner Environmental Systems* 6:100094
- Jia ZX, Wang F, Wang ZL (2019) Adsorption kinetics and thermodynamics of bisphenol A on cypress branches biochar. *J Tianjin Normal Univ (Nat Sci Ed)* 39(1):38–45
- Li L, Zhang H, Liu Z, Su Y, Du C (2023a) Adsorbent biochar derived from corn stalk core for highly efficient removal of bisphenol A. *Environ Sci Pollut Res* 30(30):74916–74927
- Li S, Hu J, Aryee AA, Sun Y, Li Z (2023b) Three birds, one stone: disinfecting and turning waste medical masks into valuable carbon dots for sodium hydrosulfite and Fe³⁺ detection enabled by a simple hydrothermal treatment. *Spectrochim Acta Part A Mol Biomol Spectrosc* 296:122659
- Lu J, Zhang C, Wu J, Luo Y (2017) Adsorptive removal of bisphenol A using N-doped biochar made of *Ulva prolifera*. *Water Air Soil Pollut* 228(9):327
- Luo Z, Zhu X, Deng J, Gong K, Zhu X (2021) High-value utilization of mask and heavy fraction of bio-oil: from hazardous waste to biochar, bio-oil, and graphene films. *J Hazard Mater* 420:126570

- Mpatani FM, Han R, Aryee AA, Kani AN, Li Z, Qu L (2021) Adsorption performance of modified agricultural waste materials for removal of emerging micro-contaminant bisphenol A: a comprehensive review. *Sci Total Environ* 780:146629
- Oginni O (2022) COVID-19 disposable face masks: a precursor for synthesis of valuable bioproducts. *Environ Sci Pollut Res Int* 29(57):85574–85576
- Pan J, Zhang YX, Yang M, Wang SY, Li L, Huang LL (2022) Adsorption properties of BPA in aqueous solution by modified biochar. *J Shenyang Normal Univ (Nat Sci Ed)* 40(6):520–526
- Qiang Y, Liu Q, Wang Y, Li M, Wang T, Zheng J (2023) Characteristics and mechanism of tetracycline adsorption from N, S Co-doped activated carbon spheres. *J Environ Sci* 43(05):249–260
- Qu J, Dong M, Wei S, Meng Q, Hu L, Hu Q, Wang L, Han W, Zhang Y (2020) Microwave-assisted one pot synthesis of β -cyclodextrin modified biochar for concurrent removal of Pb(II) and bisphenol a in water. *Carbohyd Polym* 250:117003
- Saberian M, Li J, Kilmartin-Lynch S, Boroujeni M (2021) Repurposing of COVID-19 single-use face masks for pavements base/subbase. *Sci Total Environ* 769(112):145527
- Shi W, Wang H, Yan J, Shan L, Quan G, Pan X, Cui L (2022) Wheat straw derived biochar with hierarchically porous structure for bisphenol A removal: preparation, characterization, and adsorption properties. *Sep Purif Technol* 289:120796
- Song ZF, Shi XQ, Liu Z, Song D, Cao N, Mo YK, Zhao SJ, Zhao CJ, Yang YS (2020) Synthesis and characterization of reed-based biochar and its adsorption properties for Cu^{2+} and bisphenol A(BPA). *Environ Chem* 39(8):2196–2205
- Tang Y, Li Y, Zhan L, Wu D, Zhang S, Pang R, Xie B (2022) Removal of emerging contaminants (bisphenol A and antibiotics) from kitchen wastewater by alkali-modified biochar. *Sci Total Environ* 805:150158
- Wang T, Husein DZ (2023) Novel synthesis of multicomponent porous nano-hybrid composite, theoretical investigation using DFT and dye adsorption applications: disposing of waste with waste. *Environ Sci Pollut Res* 30(4):8928–8955
- Wang T, Ma J, Qu D, Zhang X, Zheng J, Zhang X (2017) Characteristics and mechanism of copper adsorption from aqueous solutions on biochar produced from sawdust and apple branch. *Environ Sci* 38(5):2161–2171
- Wang T, Li G, Yang K, Zhang X, Wang K, Cai J, Zheng J (2021a) Enhanced ammonium removal on biochar from a new forestry waste by ultrasonic activation: characteristics, mechanisms and evaluation. *Sci Total Environ* 778:146295
- Wang T, Zheng J, Liu H, Peng Q, Zhou H, Zhang X (2021b) Adsorption characteristics and mechanisms of Pb^{2+} and Cd^{2+} by a new agricultural waste—*Caragana korshinskii* biomass derived biochar. *Environ Sci Pollut Res* 28(11):13800–13818
- Wang C, Zou R, Lei H, Qian M, Lin X, Mateo W, Wang L, Zhang X, Ruan R (2022) Biochar-advanced thermocatalytic salvaging of the waste disposable mask with the production of hydrogen and mono-aromatic hydrocarbons. *J Hazard Mater* 426:128080
- Wang T, Shi H, Kumar A, Zhang D, Wang H, Wang S, Zheng J (2024) Efficient visible-light photocatalysis of chloramphenicol using novel engineered biochar-based Ti-doped Bi_2WO_6 composite: mechanisms, degradation pathways, and applications. *Sep Purif Technol* 332:125780
- Xu JW, Yin MN, Shi L, Zhang H (2023) Study on the efficient adsorption mechanism of bisphenol A by puffed biochar. *Environ Chem* 42(1):253–263
- Ye YC, Sun YQ, Saren G, Shi LL, Zhang Z, Wang T, Liu YH (2020) Adsorption of bisphenol a by phosphoric acid modified biochar-LDHs(Mg-Al- NO_3) composite. *Environ Chem* 39(1):61–70
- Yuwen C, Liu B, Rong Q, Zhang L, Guo S (2022) Porous carbon materials derived from discarded COVID-19 masks via microwave solvothermal method for lithium-sulfur batteries. *Sci Total Environ* 817:152995
- Zhang D, Wang T, Zhi J, Zheng Q, Chen Q, Zhang C, Li Y (2020) Utilization of Jujube biomass to prepare biochar by pyrolysis and activation: characterization, adsorption characteristics, and mechanisms for nitrogen. *Materials (basel)* 13(24):5594
- Zhang HF, Mawuli D, Wang XC, Zheng YC (2023) The adsorption characteristics of bisphenol A and sulfamethoxazole onto bamboo-based biochar wetland substrates. *Technol Water Treat* 49(4):67–72+77

Publisher's Note Springer Nature remains neutral with regard to jurisdictional claims in published maps and institutional affiliations.

Springer Nature or its licensor (e.g. a society or other partner) holds exclusive rights to this article under a publishing agreement with the author(s) or other rightsholder(s); author self-archiving of the accepted manuscript version of this article is solely governed by the terms of such publishing agreement and applicable law.